

# Topology of Disconnected Elementary Band Representations

Jennifer Cano,<sup>1</sup> Barry Bradlyn,<sup>1</sup> Zhijun Wang,<sup>2</sup> L. Elcoro,<sup>3</sup> M. G. Vergniory,<sup>4,5,6</sup> C. Felser,<sup>7</sup> M. I. Aroyo,<sup>3</sup> and B. Andrei Bernevig<sup>2,4,8,9,10,\*</sup>

<sup>1</sup>*Princeton Center for Theoretical Science, Princeton University, Princeton, New Jersey 08544, USA*

<sup>2</sup>*Department of Physics, Princeton University, Princeton, New Jersey 08544, USA*

<sup>3</sup>*Department of Condensed Matter Physics, University of the Basque Country UPV/EHU, Apartado 644, 48080 Bilbao, Spain*

<sup>4</sup>*Donostia International Physics Center, P. Manuel de Lardizabal 4, 20018 Donostia-San Sebastián, Spain*

<sup>5</sup>*Department of Applied Physics II, University of the Basque Country UPV/EHU, Apartado 644, 48080 Bilbao, Spain*

<sup>6</sup>*Ikerbasque, Basque Foundation for Science, 48013 Bilbao, Spain*

<sup>7</sup>*Max Planck Institute for Chemical Physics of Solids, 01187 Dresden, Germany*

<sup>8</sup>*Laboratoire Pierre Aigrain, Ecole Normale Supérieure-PSL Research University, CNRS, Université Pierre et Marie Curie-Sorbonne Universités,*

*Université Paris Diderot-Sorbonne Paris Cité, 24 rue Lhomond, 75231 Paris Cedex 05, France*

<sup>9</sup>*Sorbonne Universités, UPMC Univ Paris 06, UMR 7589, LPTHE, F-75005, Paris, France*

<sup>10</sup>*LPTMS, CNRS (UMR 8626), Université Paris-Saclay, 15 rue Georges Clémenceau, 91405 Orsay, France*

(Dated: July 10, 2018)

Elementary band representations are the fundamental building blocks of atomic limit band structures. They have the defining property that at partial filling they cannot be both gapped and trivial. Here, we give two examples – one each in a symmorphic and a non-symmorphic space group – of elementary band representations realized with an energy gap. In doing so, we explicitly construct a counterexample to a claim by Michel and Zak that single-valued elementary band representations in non-symmorphic space groups with time-reversal symmetry are connected. For each example, we construct a topological invariant to explicitly demonstrate that the valence bands are non-trivial. We discover a new topological invariant: a movable but unremovable Dirac cone in the “Wilson Hamiltonian” and a bent- $\mathbb{Z}_2$  index.

The theory of topological quantum chemistry introduced in Ref. 1 diagnoses topological phases based on elementary band representations. A set of bands is topological if it lacks an “atomic limit” that obeys the crystal symmetry (and time-reversal, if desired): formally, an atomic limit exhibits a set of localized, symmetric Wannier functions.[1–7] This definition includes all known topological insulating phases.[8–18] We showed in Refs. 1 and 2 that each atomic limit defines a “band representation,” which is a representation of the full space group. The irreducible representations (irreps) of the little group at each point in the Brillouin zone are completely determined for each band representation.[19–21] However, the little group irreps do not define the band representation: two groups of bands can exhibit the same little group irreps but differ by a Berry phase.[2, 22–24]

If a set of bands, separated by an energy gap from all other bands, does not transform as a band representation, it does not have localized, symmetric Wannier functions; consequently, it is topological.[1, 2] An “elementary” band representation (EBR) is not equivalent to a sum of two band representations. It follows that a disconnected (gapped) elementary band representation must realize a set of topological bands.[1–3] Such disconnected EBRs will be the focus of this letter. All EBRs and their irreps at high-symmetry points in the Brillouin zone can be found on the Bilbao Crystallographic Server.[1, 25–30]

The theory of topological quantum chemistry also

brings to light the different types of trivial-to-topological phase transitions, distinguished by how many symmetry-distinct orbitals contribute to the topological bands. For example, the Kane-Mele model of graphene[8] requires only one type of symmetry-distinct orbital (the two spinful  $p_z$  orbitals per unit cell are related by the honeycomb lattice symmetry), while the trivial-to-topological transition in HgTe[13] requires both  $s$  and  $p$  orbitals to create a “band inversion.” These two types of topological insulators differ in their atomic limit as the distance between atoms is taken to infinity: in the atomic limit of graphene, the band structure consists of a single flat and four-fold degenerate band, corresponding to a single EBR. In contrast, in HgTe, the atomic limit will consist of two flat bands, one each for the  $s$  and  $p$  orbitals, corresponding to two distinct EBRs.

In this letter, we will focus on the graphene-like case: topological insulators that derive from a single orbital and its symmetry-related partners. In the language of band representations, the conduction and valence bands together transform as a single EBR; consequently, either the conduction or valence bands (or both) lack an atomic limit and are topological.[1–3]

We introduce models in a symmorphic and a non-symmorphic space group. The symmorphic example describes  $p_{x,y}$  orbitals on the honeycomb lattice. Without spin-orbit coupling (SOC), the band structure can be a (gapped) topological crystalline insulator (TCI). With infinitesimal SOC and time-reversal symmetry, the sys-

tem exhibits a nontrivial  $\mathbb{Z}_2$  index.

We were motivated to explore the non-symmorphic example because, as part of their ground-breaking work on the connectivity of energy bands, Michel and Zak conjectured that spinless EBRs in non-symmorphic space groups cannot realize a gapped band structure.[31, 32] In Ref 26, we explained where Michel and Zak’s proof fails. Here, we pick a particular non-symmorphic space group,  $P4_232$ , and construct a tight-binding model to explicitly show its gapped, topological nature. In doing so, we find a novel feature: the two-dimensional “Wilson Hamiltonian” exhibits a topologically protected band crossing.

In each example, we derive a bulk topological invariant. An essential tool is the “ $k_{\parallel}$ -directed” Wilson loop, which describes the parallel transport of an isolated set of bands:[4, 17, 33–42]

$$\mathcal{W}_{(k_{\perp}, k_0)} \equiv P e^{i \int_{k_0}^{k_0+2\pi} dk_{\parallel} A_{\parallel}(k_{\perp}, k_{\parallel})}, \quad (1)$$

where  $P$  indicates that the integral is path-ordered and  $A_{\parallel}(\mathbf{k})_{ij} = i \langle u_i(\mathbf{k}) | \partial_{k_{\parallel}} u_j(\mathbf{k}) \rangle$  is a matrix whose rows and columns correspond to each eigenstate in the isolated set of bands. The eigenvalues of  $\mathcal{W}$  are gauge invariant and of the form  $e^{i\theta(k_{\perp})}$ , independent of the “base point,”  $k_0$ . [40] A quantized invariant derived from the Wilson loop is invariant under any deformation of the Hamiltonian that preserves the gap in the spectrum.

*Spinless TCI on the honeycomb lattice* We start with spinless  $p_{x,y}$  orbitals on the honeycomb lattice, described by the nearest-neighbor Hamiltonian: [43]

$$H_{\mathbf{k}}^0 = \begin{pmatrix} 0 & h_{\mathbf{k}} \\ h_{\mathbf{k}}^{\dagger} & 0 \end{pmatrix} \quad (2)$$

where non-zero blocks mix the  $A$  and  $B$  sublattices and

$$\begin{aligned} h_{\mathbf{k}} = & \frac{1}{2} (e^{-i\mathbf{k}\cdot\delta_1} + e^{-i\mathbf{k}\cdot\delta_2} + e^{-i\mathbf{k}\cdot\delta_3}) (t_{\sigma} + t_{\pi}) \mathbb{I} \\ & + \frac{1}{2} \left( e^{-i\mathbf{k}\cdot\delta_1} - \frac{1}{2} e^{-i\mathbf{k}\cdot\delta_2} - \frac{1}{2} e^{-i\mathbf{k}\cdot\delta_3} \right) (t_{\sigma} - t_{\pi}) \sigma_z \\ & + \frac{\sqrt{3}}{4} (e^{-i\mathbf{k}\cdot\delta_2} - e^{-i\mathbf{k}\cdot\delta_3}) (t_{\sigma} - t_{\pi}) \sigma_x \end{aligned} \quad (3)$$

The Pauli matrices,  $\sigma_{x,y,z}$ , act in the  $p_{x,y}$  subspace;  $t_{\sigma,\pi}$  parameterize  $\sigma$  and  $\pi$  bond strengths; and  $\delta_{1,2,3}$  are the nearest-neighbor vectors (see Fig 1a). Previously this model with  $t_{\pi} = 0$  was studied for its flat bands.[44, 45] The spectrum of  $H_{\mathbf{k}}^0$  is shown in Fig 1b. The degeneracies at  $K \equiv \frac{2}{3}\mathbf{g}_1 + \frac{1}{3}\mathbf{g}_2$  and  $\Gamma$  are symmetry-required.[46]

To open a gap, we add the following next-nearest neighbor hopping term, which preserves the crystal symmetries of the honeycomb lattice:[47]

$$H_{\mathbf{k}}^1 = \sin(\frac{1}{2}\mathbf{k}\cdot\mathbf{e}_1) \sin(\frac{1}{2}\mathbf{k}\cdot\mathbf{e}_2) \sin(\frac{1}{2}\mathbf{k}\cdot(\mathbf{e}_1 - \mathbf{e}_2)) \tau_z \otimes \sigma_y, \quad (4)$$

where the matrices  $\tau_i$  act in the sublattice subspace. The term in Eq. (4) changes the energy-ordering of the bands

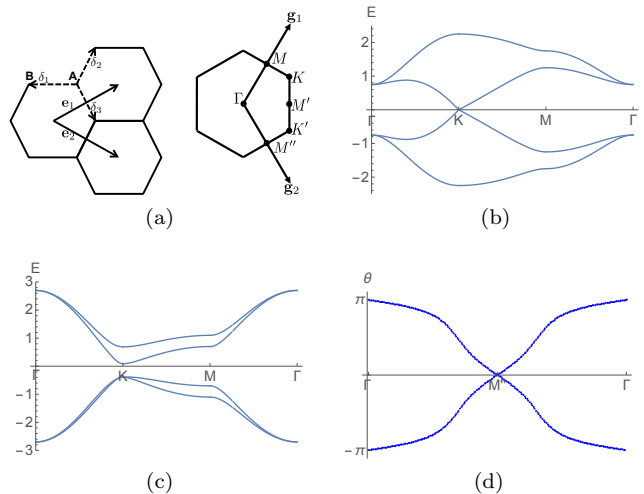


FIG. 1. (a) Lattice ( $\mathbf{e}_{1,2}$ ) and reciprocal lattice ( $\mathbf{g}_{1,2}$ ) basis vectors. The dotted arrows ( $\delta_{1,2,3}$ ) indicate the vectors between nearest neighbor sites.  $\mathbf{A}$  and  $\mathbf{B}$  indicate the sublattices. (b) Spectrum of  $H_{\mathbf{k}}^0$  with  $t_{\sigma} = 1, t_{\pi} = -.5$  (c) Gapped band structure of  $H_{\mathbf{k}}^0 + xH_{\mathbf{k}}^1$  with  $t_{\sigma} = .8, t_{\pi} = 1.0, x = .6$  and (d) the argument of its Wilson loop eigenvalues.

at  $K$ , while preserving the two-fold degeneracy. For large enough  $|x|$ ,  $H_{\mathbf{k}}^0 + xH_{\mathbf{k}}^1$  can be gapped, as in Fig. 1c; see Sec. S1A for a phase diagram.

The spectrum in Fig 1c represents a disconnected EBR.[1, 2] We construct a non-trivial bulk topological invariant from the  $\mathbf{g}_1$ -directed Wilson loop of the lower two bands. Its eigenvalues are shown in Fig. 1d as a function of the base point. When the base point is  $\Gamma$  or  $M$ , the Wilson loop eigenvalues ( $-1$  and  $+1$ , respectively[48]) are completely determined by the  $C_{2z}$  eigenvalues[38, 42] (the  $C_{2z}$  operator is  $-\tau_x \otimes \sigma_0$ . [49]) This forces the “Wilson bands” to wind in opposite directions. The quantized eigenvalues at  $\Gamma$  and  $M$  prevent the Wilson spectrum from being smoothly deformed to flat, which indicates that the valence bands are topologically nontrivial.

The Wilson loop winding requires that both occupied bands of  $H_{\mathbf{k}}^0 + xH_{\mathbf{k}}^1$  at  $\Gamma$  have the same  $C_{2z}$  eigenvalue,  $\eta$ , and that both occupied bands at  $M$  have the  $C_{2z}$  eigenvalue  $-\eta$ . Consider the Wilson loop of three bands: the two occupied bands and a third, trivial, band, not in our model. If the  $C_{2z}$  eigenvalues of the third band at  $\Gamma$  and  $M$  are both equal to  $\eta$ , then the eigenvalues of the three-band Wilson loop will not be quantized at  $M$  and it will fail to wind. Thus, the topological invariant is not stable to adding a third band to the projector (although the winding of the projector onto two bands is invariant under adding a third band as long as the gap between the third band and the existing bands does not close.) The existence of a topological invariant that depends on the number of bands is reminiscent of the “Hopf insulator.” [50]

*Spinful topological phases* We now consider SOC. Spinful  $p_{x,y}$  orbitals decompose into three irreps of the site-symmetry group. Bands derived from these three irreps transform as a sum of three EBRs,[1, 2] which generically split into four sets of disconnected bands, as in Figs 2a and 2b. At least one set of disconnected bands is either an obstructed atomic limit – it can be adiabatically deformed to a Hamiltonian comprised of orbitals that reside at the center of the hexagon rather than the corners – or a topological band that does not have any atomic limit.[51]

If time-reversal symmetry is enforced, we can consider the  $\mathbb{Z}_2$  index. For small spin-conserving SOC that does not invert the bands at  $\Gamma$  or  $M$ , the  $C_{2z}$  eigenvalues in the spinless phase determine the  $\mathbb{Z}_2$  index of each set of bands (conserving spin amounts to enforcing inversion symmetry.) Our simple, but physically motivated, model yields two phases, shown in Fig 2: either all three or the first/third gaps are  $\mathbb{Z}_2$  topological, while the middle gap is not; there is no phase in which all gaps are  $\mathbb{Z}_2$  trivial.[52] We show in Sec. SIC that only spin-conserving SOC can open a gap in the spinless band structure; hence, if non-spin-conserving SOC is present and does not invert any bands, it will alter the band structure but not change the  $\mathbb{Z}_2$  index.

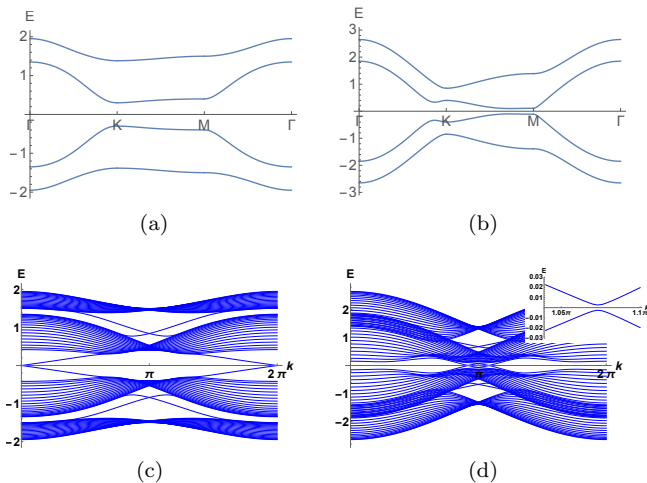


FIG. 2. Band structures with an onsite  $L \cdot S$  term for (a,b) periodic and (c,d) slab boundary conditions. This SOC term preserves inversion symmetry, such that all bands remain doubly degenerate, but is general enough to open all possible gaps in the band structure. In (a) only the lowest and highest bands have a nontrivial  $\mathbb{Z}_2$  index and hence the slab boundary conditions in (c) reveal edge states in all three gaps. In (b) all four bands have a nontrivial  $\mathbb{Z}_2$  index and hence the slab boundary conditions in (d) reveal edge states in only the upper and lower gaps. The inset in (d) resolves the avoided crossing at  $E = 0$ .

*Material realization* The spinless semi-metallic model  $H_{\mathbf{k}}^0$  consists of nearest-neighbor Slater-Koster[53] terms; thus, it is widely applicable to two-dimensional planar

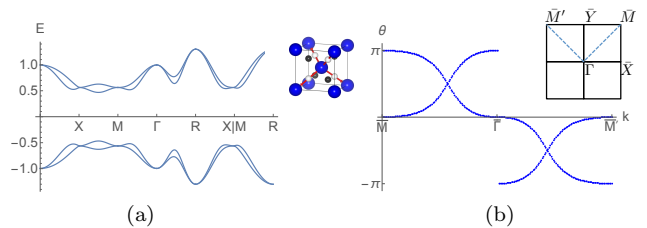


FIG. 3. (a) Spectrum of  $H_{\mathbf{k}} + H_{\mathbf{k}}^1$  with  $t_1 = .2, t_2 = .3, t_3 = .1, t_4 = .08, t_5 = .05, t_6 = .02$ . Inset shows unit cell: orbitals on the blue atoms enter the Hamiltonian, while the white/black atoms create a crystal field with the symmetry of  $P4_232$ . (b) Argument of the eigenvalues of the  $z$ -directed Wilson matrix along the path  $\bar{M} - \bar{\Gamma} - \bar{M}'$  (blue dotted line in inset);  $\bar{M} = (\pi, \pi)$ ,  $\bar{\Gamma} = (0, 0)$ ,  $\bar{M}' = (-\pi, \pi)$ .

honeycomb systems. To exhibit the TCI phase, the next-nearest neighbor term,  $H_{\mathbf{k}}^1$ , must be dominant in order to open a gap. The relative strength of the hopping terms varies with strain or buckling.

The non-trivial  $\mathbb{Z}_2$  phases will be present whenever SOC is large enough to open an observable gap, but not so large to invert the bands at  $\Gamma$  and  $M$ . In particular,  $H_{\mathbf{k}}^0$  with SOC describes bismuth grown on an SiC substrate, consistent with the topological edge states reported in Ref 54.

*Non-symmorphic gapped EBR* We now consider the non-symmorphic simple cubic space group  $P4_232$ , which is generated by  $\{C_{2x}|\mathbf{0}\}$ ,  $\{C_{3,111}|\mathbf{0}\}$  and  $\{C_{2,110}|\frac{1}{2}\frac{1}{2}\frac{1}{2}\}$ . We also enforce time-reversal symmetry. We consider atoms sitting at  $(0, 0, 0)$  and  $(\frac{1}{2}, \frac{1}{2}, \frac{1}{2})$  (inset to Fig 3a), which together comprise the  $2a$  Wyckoff position, each with spinless  $d_{z^2}$  and  $d_{x^2-y^2}$  orbitals, which together form a time-reversal symmetric irrep of the site-symmetry group.[55, 56] Since the orbitals transform as an irrep of a maximal Wyckoff position, any band structure derived from these orbitals transforms as a time-reversal invariant EBR. It follows from Ref 2 that if the band structure is gapped, it contains topological bands. Here, we explicitly construct a gapped Hamiltonian and a nontrivial bulk topological invariant, violating the conjecture[31, 32] that a single set of symmetry-related orbitals in a non-symmorphic space group always yields a gapless band structure.

We consider the following Hamiltonian, which respects all space group symmetries and time-reversal:[57]

$$H_{\mathbf{k}} = t_1 f_1(\mathbf{k}) \tau_x \otimes \sigma_0 + t_2 f_2(\mathbf{k}) \tau_y \otimes \sigma_0 + t_3 (g_1(\mathbf{k}) \tau_z \otimes \sigma_z + g_2(\mathbf{k}) \tau_z \otimes \sigma_x), \quad (5)$$

where  $f_1(\mathbf{k}) = \sum_i \cos(\mathbf{k} \cdot \delta_i)$ ,  $f_2(\mathbf{k}) = \sum_i \sin(\mathbf{k} \cdot \delta_i)$ ,  $g_1(\mathbf{k}) = \cos k_x - \cos k_y$ ,  $g_2(\mathbf{k}) = (\cos k_x + \cos k_y - 2 \cos k_z) / \sqrt{3}$  and  $\delta_{1,2,3,4}$  are vectors to nearest neighbors, shown in Fig 3a. The band structure is doubly-degenerate and gapped when  $t_{1,2,3} \neq 0$ . To eliminate the extra degen-

eracies, we add the symmetry-preserving term

$$H_{\mathbf{k}}^1 = t_4 f_1(\mathbf{k}) \tau_y \otimes \sigma_y + t_5 \tau_0 \otimes (g_2(\mathbf{k}) \sigma_z - g_1(\mathbf{k}) \sigma_x) + t_6 g_3(\mathbf{k}) \tau_z \otimes \sigma_0, \quad (6)$$

where

$$g_3(\mathbf{k}) = \cos(2k_x) \cos(k_y) - \cos(2k_y) \cos(k_x) + \text{perm.} \quad (7)$$

and ‘+ perm’ indicates terms obtained by permuting  $k_x \rightarrow k_y \rightarrow k_z$ . The spectrum of  $H_{\mathbf{k}} + H_{\mathbf{k}}^1$  is shown in Fig 3a. Since  $H_{\mathbf{k}}$  is fully gapped when  $t_{1,2,3} \neq 0$ ,  $H_{\mathbf{k}} + H_{\mathbf{k}}^1$  is gapped when  $t_{4,5,6}$  are small compared to  $t_{1,2,3}$ .

This gapped phase realizes a disconnected and time-reversal symmetric EBR; thus, it contains topological bands. We diagnose the topological phase by the winding of its  $z$ -directed Wilson loop along the *bent* path shown in Fig 3b. This is a time-reversal symmetric and non-symmorphic generalization of the ‘‘bent Chern number’’ introduced in Ref 58. Two features are necessary for this loop to wind: first, the Wilson loop eigenvalues are pinned to  $\pm 1$  at  $\bar{\Gamma}$  and  $\bar{M}$ , and, second, there are protected band crossings in the Wilson spectrum along the  $|k_x| = |k_y|$  lines. Combined, these features prevent the Wilson bands from being smoothly deformable to flat bands; hence, the phase is topological.

We now explain the origin of these features: first,  $C_{2x}$  symmetry forces the eigenvalues of  $\mathcal{W}_{(\bar{\Gamma},0)}$  and  $\mathcal{W}_{(\bar{M},0)}$  to be real, while the  $\{C_{2,110}|\frac{1}{2}\frac{1}{2}\frac{1}{2}\}$  screw symmetry forces them to come in pairs  $(\lambda, -\lambda^*)$ . [59] This combination pins the eigenvalues of  $\mathcal{W}_{(k_x, k_y, 0)}$  to be  $\pm 1$  at  $\bar{\Gamma}$  and  $\bar{M}$ .

The Wilson band crossing is subtle: the  $\{C_{2,110}|\frac{1}{2}\frac{1}{2}\frac{1}{2}\}$  screw symmetry requires the eigenvalues of  $\mathcal{W}_{(k,k,0)}$  to come in pairs  $(\lambda, -\lambda^*)$ . Combined with the anti-unitary symmetry  $\mathcal{T}\{C_{2,110}|\frac{1}{2}\frac{1}{2}\frac{1}{2}\}^{-1}C_{2z}$ , which leaves points  $(k, k, k_z)$  invariant, the Wilson matrix must take the form  $\mathcal{W}_{(k,k,0)} = i e^{i a_x(k) \sigma_x + i a_y(k) \sigma_y}$ , where, importantly,  $a_x(k) \propto a_y(k)$  (alternately, the symmetries permit the eigenvalues of  $\mathcal{W}_{(k,k,0)}$  to be fixed to  $\pm 1$ ; see Sec. S3B.) Then degeneracies of the Wilson eigenvalues, which occur when  $a_x(k) = a_y(k) = 0$ , are not fine-tuned, since the symmetry forced  $a_x(k) \propto a_y(k)$ . Since the eigenvalues of  $\mathcal{W}_{(k,k,0)}$  at  $k = 0$  and  $k = \pi$  are fixed to  $+1$  and  $-1$ , an odd number of linear degeneracies between  $\bar{\Gamma}$  and  $\bar{M}$  cannot be removed without closing the bulk band gap. Thus, the parity of the number of linear degeneracies is a topological invariant.

The band crossing forms a Dirac cone in the two-dimensional ‘‘Wilson Hamiltonian.’’ [40] The Dirac point is revealed by the Berry phase,  $w$ , acquired by an eigenstate of  $\mathcal{W}_{(k_x, k_y, 0)}$  as it traverses the path  $\gamma$  around the Dirac point. The Berry phase of Wilson loop eigenstates was introduced in Ref. 41. Since  $w$  is quantized to  $\pm 1$  (see Sec. S4), it constitutes a topological invariant. In our model, for several values of parameters, we have numerically computed the nontrivial value,  $w = -1$ .

When SOC is present, the spinful  $d_{z^2}$  and  $d_{x^2-y^2}$  orbitals transform as spin- $\frac{3}{2}$  orbitals, which induce an eight-band time-reversal symmetric EBR. [27] When the EBR is gapped, the valence (or conduction) bands must be topological.

*Weak symmetry indicators* In both the spinless TCI on the honeycomb lattice and the non-symmorphic gapped EBR, the valence bands are topological, but have the property that the irreps at high-symmetry points can be written as a ‘‘difference’’ of the irreps in two other EBRs. [60] Because the irreps can be written as a difference, classification schemes [61] that treat the little group irreps as a vector space will identify the valence bands as trivial, even though they lack an atomic limit. However, unless an energy gap closes to the valence bands, the winding of the Wilson loop in both examples provides a robust and quantized topological invariant that is, in principle, physically observable. [42, 62, 63]

This distinction warrants a refined characterization of topological crystalline bands based on whether their topological nature can be deduced by their little group irreps. We label the symmetry properties of topological bands as strong if their little group irreps are not equal to a linear combination of little group irreps corresponding to EBRs and weak if their little group irreps are equal to a difference (but not a sum) of irreps in EBRs. Strong symmetry properties implies a stable topological index; however, the converse is not true: for example, bands with a nontrivial  $\mathbb{Z}_2$  index under time-reversal symmetry can be strong [10] or weak. [1] This usage of weak and strong symmetry is different than the current distinction between weak and strong topological insulators. [10] It is more suitable for the refined classification of topological insulators with crystal symmetries.

*Conclusions* We have constructed tight-binding models to realize the insulating phases of two gapped EBRs. We explicitly showed that the valence bands have a nontrivial topological invariant. In doing so, we found a new topological invariant in a non-symmorphic space group: a Dirac cone in the Wilson loop spectrum and a Wilson loop that winds along a bent path. This motivates further study of the gapped EBRs in other non-symmorphic space groups. In addition, we introduced the notion of a weak symmetry indicator. We postpone a general investigation of the symmetry properties of gapped EBRs to future work.

*Acknowledgments* BB, JC, ZW, and BAB acknowledge the hospitality of the Donostia International Physics Center. BAB acknowledges the hospitality and support of the École Normale Supérieure and Laboratoire de Physique Théorique et Hautes Energies. The work of MGW was supported by FIS2016-75862-P. The work of LE and MIA was supported by the Government of the Basque Country (project IT779-13) and the Spanish Ministry of Economy and Competitiveness and FEDER funds (project MAT2015-66441-P). BAB acknowledges

the support of the NSF EAGER Award DMR – 1643312, ONR - N00014-14-1-0330, NSF-MRSEC DMR-1420541, ARO MURI W911NF-12-1-0461, the Department of Energy de-sc0016239, the Simons Investigator Award, Packard Foundation and the Schmidt Fund for Innovative Research.

---

\* Permanent Address: Department of Physics, Princeton University, Princeton, New Jersey 08544, USA

- [1] B. Bradlyn, L. Elcoro, J. Cano, M. G. Vergniory, Z. Wang, C. Felser, M. I. Aroyo, and B. A. Bernevig, *Nature* **547**, 298 (2017), arXiv:1703.02050 [cond-mat].
- [2] J. Cano, B. Bradlyn, Z. Wang, L. Elcoro, M. G. Vergniory, C. Felser, M. I. Aroyo, and B. A. Bernevig, *Phys. Rev. B* **97**, 035139 (2018), arXiv:1709.01935 [cond-mat].
- [3] H. C. Po, H. Watanabe, and A. Vishwanath, (2017), arXiv:1709.06551.
- [4] A. A. Soluyanov and D. Vanderbilt, *Phys. Rev. B* **83**, 035108 (2011).
- [5] A. A. Soluyanov and D. Vanderbilt, *Phys. Rev. B* **85**, 115415 (2012).
- [6] N. Marzari, A. A. Mostofi, J. R. Yates, I. Souza, and D. Vanderbilt, *Rev. Mod. Phys.* **84**, 1419 (2012).
- [7] N. Read, *Phys. Rev. B* **95**, 115309 (2017).
- [8] C. L. Kane and E. J. Mele, *Phys. Rev. Lett.* **95**, 226801 (2005).
- [9] J. E. Moore and L. Balents, *Phys. Rev. B* **75**, 121306 (2007).
- [10] L. Fu and C. L. Kane, *Phys. Rev. B* **76**, 045302 (2007).
- [11] L. Fu, C. L. Kane, and E. J. Mele, *Phys. Rev. Lett.* **98**, 106803 (2007).
- [12] R. Roy, *Phys. Rev. B* **79**, 195322 (2009).
- [13] B. A. Bernevig, T. L. Hughes, and S.-C. Zhang, *Science* **314**, 1757 (2006), <http://science.sciencemag.org/content/314/5806/1757.full.pdf>
- [14] J. C. Y. Teo, L. Fu, and C. L. Kane, *Phys. Rev. B* **78**, 045426 (2008).
- [15] L. Fu, *Phys. Rev. Lett.* **106**, 106802 (2011).
- [16] K. Shiozaki, M. Sato, and K. Gomi, *Phys. Rev. B* **95**, 235425 (2017).
- [17] B. J. Wieder, B. Bradlyn, Z. Wang, J. Cano, Y. Kim, H.-S. D. Kim, A. M. Rappe, C. L. Kane, and B. A. Bernevig, (2017), arXiv:1705.01617.
- [18] H. Song, S.-J. Huang, L. Fu, and M. Hermele, *Phys. Rev. X* **7**, 011020 (2017).
- [19] J. Zak, *Phys. Rev. Lett.* **45**, 1025 (1980).
- [20] J. Zak, *Phys. Rev. B* **26**, 3010 (1982).
- [21] H. Bacry, L. Michel, and J. Zak, "Symmetry and classification of energy bands in crystals," in *Group theoretical methods in Physics: Proceedings of the XVI International Colloquium Held at Varna, Bulgaria, June 15–20 1987* (Springer Berlin Heidelberg, 1988) p. 289.
- [22] H. Bacry, L. Michel, and J. Zak, *Phys. Rev. Lett.* **61**, 1005 (1988).
- [23] H. Bacry, *Commun. Math. Phys.* **153**, 359 (1993).
- [24] L. Michel and J. Zak, *EPL (Europhysics Letters)* **18**, 239 (1992).
- [25] B. Bradlyn, L. Elcoro, M. G. Vergniory, J. Cano, Z. Wang, C. Felser, M. I. Aroyo, and B. A. Bernevig, *Phys. Rev. B* **97**, 035138 (2018), arXiv:1709.01937.
- [26] M. G. Vergniory, L. Elcoro, Z. Wang, J. Cano, C. Felser, M. I. Aroyo, B. A. Bernevig, and B. Bradlyn, *Phys. Rev. E* **96**, 023310 (2017), arXiv:1706.08529.
- [27] L. Elcoro, B. Bradlyn, Z. Wang, M. G. Vergniory, J. Cano, C. Felser, B. A. Bernevig, D. Orobengoa, G. de la Flor, and M. I. Aroyo, *Journal of Applied Crystallography* **50**, 1457 (2017), arXiv:1706.09272.
- [28] M. I. Aroyo, J. M. Perez-Mato, D. Orobengoa, E. Tasci, G. de la Flor, and A. Kirov, *Bulg. Chem. Commun.* **43(2)**, 183 (2011).
- [29] M. I. Aroyo, J. M. Perez-Mato, C. Capillas, E. Kroumova, S. Ivantchev, G. Madariaga, A. Kirov, and H. Wondratschek, *Z. Krist.* **221**, 15 (2006).
- [30] M. I. Aroyo, A. Kirov, C. Capillas, J. M. Perez-Mato, and H. Wondratschek, *Acta Cryst.* **A62**, 115 (2006).
- [31] L. Michel and J. Zak, *Phys. Rev. B* **59**, 5998 (1999).
- [32] L. Michel and J. Zak, *Phys. Rep.* **341**, 377 (2001).
- [33] J. Zak, *Phys. Rev. Lett.* **62**, 2747 (1989).
- [34] L. Fu and C. L. Kane, *Phys. Rev. B* **74**, 195312 (2006).
- [35] S. Ryu, C. Mudry, H. Obuse, and A. Furusaki, *New Journal of Physics* **12**, 065005 (2010).
- [36] R. Yu, X. L. Qi, A. Bernevig, Z. Fang, and X. Dai, *Phys. Rev. B* **84**, 075119 (2011).
- [37] M. Taherinejad, K. F. Garrity, and D. Vanderbilt, *Physical Review B* **89**, 115102 (2014).
- [38] A. Alexandradinata, X. Dai, and B. A. Bernevig, *Physical Review B* **89**, 155114 (2014).
- [39] Z. Wang, A. Alexandradinata, R. J. Cava, and B. A. Bernevig, *Nature* **532**, 189 (2016).
- [40] A. Alexandradinata, Z. Wang, and B. A. Bernevig, *Phys. Rev. X* **6**, 021008 (2016).
- [41] W. A. Benalcazar, B. A. Bernevig, and T. L. Hughes, *Science* **357**, 61 (2017), arXiv:1611.07987.
- [42] J. Höller and A. Alexandradinata, (2017), arXiv:1708.02943.
- [43] Eqs. (2) and (3) are derived in Sec. S1.
- [44] C. Wu, D. Bergman, L. Balents, and S. Das Sarma, *Phys. Rev. Lett.* **99**, 070401 (2007).
- [45] Z. Liu, Z.-F. Wang, J.-W. Mei, Y.-S. Wu, and F. Liu, *Phys. Rev. Lett.* **110**, 106804 (2013).
- [46] E. Kogan and V. U. Nazarov, *Phys. Rev. B* **85**, 115418 (2012).
- [47] The crystal symmetries of the honeycomb lattice are enumerated in Sec. S1.
- [48] Sec. S1A shows the possible  $C_{2z}$  eigenvalues.
- [49] The crystal symmetries of the honeycomb lattice are enumerated in Sec. S1.
- [50] J. E. Moore, Y. Ran, and X.-G. Wen, *Phys. Rev. Lett.* **101**, 186805 (2008).
- [51] The possibilities are described in Sec. S1C.
- [52] The possible  $C_{2z}$  eigenvalues are computed in Sec. S1C.
- [53] J. C. Slater and G. F. Koster, *Phys. Rev.* **94**, 1498 (1954).
- [54] F. Reis, G. Li, L. Dudy, M. Bauernfeind, S. Glass, W. Hanke, R. Thomale, J. Schäfer, and R. Claessen, *Science* (2017), 10.1126/science.aai8142.
- [55] M. I. Aroyo, ed., *International Tables for Crystallography*, Vol. A (International Union of Crystallography, 2016).
- [56] S. Altmann and P. Herzig, *Point-Group Theory Tables*, 2nd ed. (University of Vienna, 2011).
- [57] Sec. S2 shows the matrix form of the symmetries.
- [58] A. Alexandradinata, C. Fang, M. J. Gilbert, and B. A. Bernevig, *Phys. Rev. Lett.* **113**, 116403 (2014).

- [59] See Sec. S3A.
- [60] Details for the honeycomb case are in Sec. S1B.
- [61] H. C. Po, A. Vishwanath, and H. Watanabe, *Nature Communications* **8**, 50 (2017), arXiv:1703.00911.
- [62] M. Atala, M. Aidelsburger, J. T. Barreiro, D. Abanin, T. Kitagawa, E. Demler, and I. Bloch, *Nature Physics* (2013).
- [63] S. Nakajima, T. Tomita, S. Taie, T. Ichinose, H. Ozawa, L. Wang, M. Troyer, and Y. Takahashi, *Nature Physics* (2016).

# Supplemental Material for Topology of Disconnected Elementary Band Representations

Jennifer Cano,<sup>1</sup> Barry Bradlyn,<sup>1</sup> Zhijun Wang,<sup>2</sup> L. Elcoro,<sup>3</sup> M. G. Vergniory,<sup>4,5,6</sup> C. Felser,<sup>7</sup> M. I. Aroyo,<sup>3</sup> and B. Andrei Bernevig<sup>2,4,8,9,10,\*</sup>

<sup>1</sup>Princeton Center for Theoretical Science, Princeton University, Princeton, New Jersey 08544, USA

<sup>2</sup>Department of Physics, Princeton University, Princeton, New Jersey 08544, USA

<sup>3</sup>Department of Condensed Matter Physics, University of the Basque Country UPV/EHU, Apartado 644, 48080 Bilbao, Spain

<sup>4</sup>Donostia International Physics Center, P. Manuel de Lardizabal 4, 20018 Donostia-San Sebastián, Spain

<sup>5</sup>Department of Applied Physics II, University of the Basque Country UPV/EHU, Apartado 644, 48080 Bilbao, Spain

<sup>6</sup>Ikerbasque, Basque Foundation for Science, 48013 Bilbao, Spain

<sup>7</sup>Max Planck Institute for Chemical Physics of Solids, 01187 Dresden, Germany

<sup>8</sup>Laboratoire Pierre Aigrain, Ecole Normale Supérieure-PSL Research University, CNRS, Université Pierre et Marie Curie-Sorbonne Universités,

Université Paris Diderot-Sorbonne Paris Cité, 24 rue Lhomond, 75231 Paris Cedex 05, France

<sup>9</sup>Sorbonne Universités, UPMC Univ Paris 06, UMR 7589, LPTHE, F-75005, Paris, France

<sup>10</sup>LPTMS, CNRS (UMR 8626), Université Paris-Saclay, 15 rue Georges Clémenceau, 91405 Orsay, France

## S1. NEAREST NEIGHBOR HAMILTONIAN FOR $p_{x,y}$ ORBITALS ON THE HONEYCOMB LATTICE

We choose the lattice basis vectors:

$$\begin{aligned} \mathbf{e}_1 &= \frac{\sqrt{3}}{2} \hat{\mathbf{x}} + \frac{1}{2} \hat{\mathbf{y}} \\ \mathbf{e}_2 &= \frac{\sqrt{3}}{2} \hat{\mathbf{x}} - \frac{1}{2} \hat{\mathbf{y}}, \end{aligned} \quad (\text{S1})$$

which are shown in Fig. 1 with their reciprocal lattice vectors,  $\mathbf{g}_i$ , which satisfy  $\mathbf{g}_i \cdot \mathbf{e}_j = 2\pi\delta_{ij}$ . Sites on the  $A(B)$  sublattice sit at positions  $\mathbf{R} + \mathbf{r}_{A(B)}$ , where  $\mathbf{R}$  denotes a lattice translation and

$$\begin{aligned} \mathbf{r}_A &= \frac{2}{3} \mathbf{e}_1 - \frac{1}{3} \mathbf{e}_2 \\ \mathbf{r}_B &= \frac{1}{3} \mathbf{e}_1 - \frac{2}{3} \mathbf{e}_2 \end{aligned} \quad (\text{S2})$$

In this basis, the symmetry generators of the honeycomb lattice act as follows:

$$\begin{aligned} C_{3z} : (\mathbf{e}_1, \mathbf{e}_2) &\rightarrow (-\mathbf{e}_2, \mathbf{e}_1 - \mathbf{e}_2) \\ C_{2z} : (\mathbf{e}_1, \mathbf{e}_2) &\rightarrow (-\mathbf{e}_1, -\mathbf{e}_2) \\ m_{1\bar{1}} : (\mathbf{e}_1, \mathbf{e}_2) &\rightarrow (\mathbf{e}_2, \mathbf{e}_1), \end{aligned} \quad (\text{S3})$$

where the subscript  $1\bar{1}$  indicates that the mirror plane has normal vector  $\mathbf{e}_1 - \mathbf{e}_2$ . For  $p_{x,y}$  orbitals, we choose the following matrix representation, in which the Pauli matrices  $\tau$  act in sublattice space and the  $\sigma$  matrices act in orbital space:

$$\begin{aligned} U_{C_{3z}} &= \tau_0 \otimes \left( -\frac{1}{2} \sigma_0 + i \frac{\sqrt{3}}{2} \sigma_y \right) \\ U_{C_{2z}} &= -\tau_x \otimes \sigma_0 \\ U_{m_{1\bar{1}}} &= \tau_0 \otimes \sigma_z, \end{aligned} \quad (\text{S4})$$

The orbital term for a rotation by an angle  $\theta$  about an axis  $\hat{\mathbf{n}}$  is represented by  $e^{i\theta\hat{\mathbf{n}} \cdot \mathbf{S}}$ , projected onto the  $p_{x,y}$  orbitals;  $\mathbf{S}$  is the vector of spin-1 matrices. A Hamiltonian,  $H_{\mathbf{k}}$ , that respects the lattice symmetry must satisfy:

$$H_{\mathbf{k}} = U_R^\dagger H_{R\mathbf{k}} U_R, \quad (\text{S5})$$

for each generator,  $R$ , of the honeycomb lattice.

Denoting the annihilation operator on site  $\mathbf{r}$  by  $c_{\mathbf{r},a}$ , where  $a = x, y$  indicates the  $p_x$  or  $p_y$  orbital, the nearest neighbor Hamiltonian is given by:

$$H = \sum_{\mathbf{R}} \sum_{a,b} \sum_{\delta_i} t_{ab}(\delta_i) c_{\mathbf{R}+\mathbf{r}_A,a}^\dagger c_{\mathbf{R}+\mathbf{r}_A+\delta_i,b} + \text{h.c.}, \quad (\text{S6})$$

where the three nearest neighbors to a site at  $\mathbf{R} + \mathbf{r}_A$  sit at  $\mathbf{R} + \mathbf{r}_A + \delta_i$  (the vectors  $\delta_i$  are depicted in Fig. 1) and  $t_{ab}(\delta_i)$  is given by one of the Slater-Koster terms:<sup>1</sup>

$$\begin{aligned} t_{xx}(\delta_i) &= \frac{1}{3} [(\delta_i \cdot \hat{\mathbf{x}})^2 t_\sigma + (\delta_i \cdot \hat{\mathbf{y}})^2 t_\pi] \\ t_{yy}(\delta_i) &= \frac{1}{3} [(\delta_i \cdot \hat{\mathbf{y}})^2 t_\sigma + (\delta_i \cdot \hat{\mathbf{x}})^2 t_\pi] \\ t_{xy}(\delta_i) &= \frac{1}{3} (\delta_i \cdot \hat{\mathbf{x}})(\delta_i \cdot \hat{\mathbf{y}})(t_\sigma - t_\pi) = t_{yx}(\delta_i), \end{aligned} \quad (\text{S7})$$

where  $t_{\sigma(\pi)}$  are free parameters that describe  $\sigma(\pi)$ -bonds. Notice that  $\mathbf{r}_A + \delta_i$  is always a site on the  $B$  sublattice. Using the Fourier transform,

$$c_{\mathbf{k},L,a} = \sum_{\mathbf{R}} e^{i\mathbf{k} \cdot (\mathbf{R} + \mathbf{r}_L)} c_{\mathbf{R} + \mathbf{r}_L, a} \quad (\text{S8})$$

where  $L = A, B$  denotes the sublattice and  $a = x, y$  denotes the orbital, the real space Hamiltonian in Eq (S6) is rewritten:

$$H = \sum_{\mathbf{k}} \sum_{a,b} \sum_{\delta_i} c_{\mathbf{k},A,a}^\dagger c_{\mathbf{k},B,b} e^{-i\mathbf{k} \cdot \delta_i} t_{ab}(\delta_i) + \text{h.c.}, \quad (\text{S9})$$

Plugging Eq (S7) into Eq (S9) yields

$$H^0 = \sum_{\mathbf{k}} \psi_{\mathbf{k}}^\dagger H_{\mathbf{k}}^0 \psi_{\mathbf{k}} \equiv \sum_{\mathbf{k}} \psi_{\mathbf{k}}^\dagger \begin{pmatrix} 0 & h_{\mathbf{k}} \\ h_{\mathbf{k}}^\dagger & 0 \end{pmatrix} \psi_{\mathbf{k}} \quad (\text{S10})$$

where  $\psi_{\mathbf{k}} = (c_{\mathbf{k},A,x} \ c_{\mathbf{k},A,y} \ c_{\mathbf{k},B,x} \ c_{\mathbf{k},B,y})^T$  contains the annihilation operators for  $p_{x,y}$  orbitals on the  $A$  and  $B$  sublattices and  $h_{\mathbf{k}}$  is given by Eq. (3).

### A. Phase diagram of $H_{\mathbf{k}}^0 + xH_{\mathbf{k}}^1$

As described in the main text, a necessary condition to reach the gapped TCI phase is that the two-fold degeneracy at  $K$  is higher or lower in energy than the other two bands. The eigenvalues of  $H_{\mathbf{k}=K}^0 + xH_{\mathbf{k}=K}^1$  are  $-\frac{3\sqrt{3}}{8}x$  (2-fold degenerate) and  $\frac{3}{8}(\pm 4(t_\pi - t_\sigma) + \sqrt{3}x)$ ; thus, the TCI phase requires:

$$|x| > \frac{2}{\sqrt{3}}|t_\pi - t_\sigma| \quad (\text{S11})$$

However, there are further constraints: band crossings along the paths connecting  $\Gamma$  and  $M$  can prevent the system from opening a gap even when the energy ordering at  $K$  allows it. Consider the two lines  $\Sigma = \alpha\mathbf{g}_1$  and  $\Lambda = \beta(\frac{1}{3}\mathbf{g}_1 + \frac{2}{3}\mathbf{g}_2)$ , which are invariant under  $C_{3z}m_{1\bar{1}}$  and  $C_{2z}C_{3z}m_{1\bar{1}}$ , respectively. As  $\alpha$  goes from 0 to  $\frac{1}{2}$ ,  $\Sigma$  connects  $\Gamma$  to  $M$ . As  $\beta$  goes from 0 to  $\frac{3}{2}$ ,  $\Lambda$  connects  $\Gamma$  to  $M+\mathbf{g}_2$  (passing through  $K'$  at  $\beta = 1$ ). We can then track the respective mirror eigenvalues along these lines to find constraints on connectivity. The BANDREP application on the BCS server shows that the  $\Gamma_5$  and  $\Gamma_6$  irreps appear at  $\Gamma$  in our model ( $p_{x,y}$  orbitals on the honeycomb correspond to the irrep  $E$  at Wyckoff position  $2b$ ). In the  $\Gamma_5$  and  $\Gamma_6$  irreps, the character of each mirror is zero: this means that the doubly-degenerate bands that comprise the  $\Gamma_5$  irrep will split into two bands along  $\Sigma$ , one of which is even under  $C_{3z}m_{1\bar{1}}$  and one of which is odd (and same for  $\Gamma_6$ ). Thus,  $\Gamma_5$  must connect to two irreps at  $M$  which have opposite parity under  $C_{3z}m_{1\bar{1}}$ . Similarly, the  $\Gamma_5$  irrep will split into two bands along  $\Lambda$ , one of which is even under  $C_{2z}C_{3z}m_{1\bar{1}}$  and one of which is odd; thus,  $\Gamma_5$  must connect to two irreps at  $M$  which have opposite parity under  $C_{2z}C_{3z}m_{1\bar{1}}$ . Without loss of generality, assume the  $\Gamma_5$  irrep is higher in energy than  $\Gamma_6$ ; then in order for the system to be an insulator, the two bands that are highest in energy at  $M$  must have opposite  $C_{3z}m_{1\bar{1}}$  eigenvalues and also opposite  $C_{2z}C_{3z}m_{1\bar{1}}$  eigenvalues.

Referring to Table S1, a gapped band structure requires one of the two following conditions to be satisfied:

$$E_{M1,M2} > E_{M3,M4} \Rightarrow 3t_\sigma < t_\pi < \frac{1}{3}t_\sigma \quad (\text{S12})$$

$$E_{M1,M2} < E_{M3,M4} \Rightarrow \frac{1}{3}t_\pi < t_\sigma < 3t_\pi \quad (\text{S13})$$

If neither Eq (S12) or (S13) is satisfied, there will be a band crossing along  $\Gamma - M$ , as shown in Fig S1a.

The  $C_{2z}$  eigenvalues at  $\Gamma$  are shown in Table S2. By comparing Table S1 with Table S2, one can check that in the gapped phase, when either Eq (S12) or (S13) is satisfied, the  $C_{2z}$  eigenvalues at  $\Gamma$  are always opposite those at  $M$  (unlike the usual time-reversal  $\mathbb{Z}_2$  invariant, here we are referring to the  $C_{2z}$  eigenvalues themselves, not their product. This guarantees that the Wilson loop in Fig. 1d always winds in the gapped phase.<sup>2</sup>

We note that it could be possible with longer range hopping terms to reach a gapped phase where the  $C_{2z}$  eigenvalues of the two lower bands at  $\Gamma$  are the same as those at  $M$  (this is symmetry-allowed according to possible decompositions of the EBR induced from  $p_{x,y}$  orbitals listed on the BCS Server<sup>3</sup>). However, this phase is not accessible within our nearest-neighbor model.

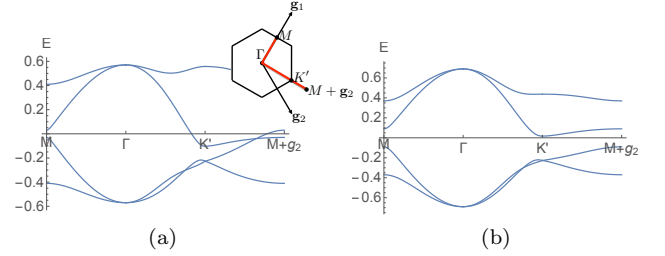


FIG. S1. Band structure of  $H_{\mathbf{k}}^0 + xH_{\mathbf{k}}^1$  along the red path shown in the inset;  $x = .35$ . In (a)  $t_\sigma = .08, t_\pi = .3$ , while in (b)  $t_\sigma = .16, t_\pi = .3$ . In both cases, Eq (S11) is satisfied; hence the band ordering at  $K$  allows for a gap. However, since the parameters in (a) violate Eq (S12) and (S13), there is a band crossing between  $\Gamma$  and  $M + \mathbf{g}_2$ . In (b), Eq (S13) is satisfied and the band structure is gapped.

Energy at $M$	$C_{3z}m_{1\bar{1}}$ eig.	$C_{2z}C_{3z}m_{1\bar{1}}$ eig.	$C_{2z}$ eig.
$E_{M1} \equiv \frac{t_\pi}{2} - \frac{3t_\sigma}{2}$	-1	1	-1
$E_{M2} \equiv -\frac{3t_\pi}{2} + \frac{t_\sigma}{2}$	1	-1	-1
$E_{M3} \equiv \frac{3t_\pi}{2} - \frac{t_\sigma}{2}$	1	1	+1
$E_{M4} \equiv -\frac{t_\pi}{2} + \frac{3t_\sigma}{2}$	-1	-1	+1

TABLE S1. Energies, mirror, and  $C_{2z}$  eigenvalues for each of the eigenstates at  $M$ . The  $C_{2z}$  eigenvalue is a product of the two mirror eigenvalues.

Energy at $\Gamma$	$C_{2z}$ eig.
$E_{\Gamma 1} = -\frac{3}{2}(t_\pi + t_\sigma)$	+1, +1
$E_{\Gamma 2} = \frac{3}{2}(t_\pi + t_\sigma)$	-1, -1

TABLE S2. Energies and  $C_{2z}$  eigenvalues for the two-fold degenerate eigenstates at  $\Gamma$ .



## B. Irreps at high-symmetry points

Using the notation on BANDREP application of the BCS<sup>3</sup>, the Hamiltonian  $H_{\mathbf{k}}^0 + xH_{\mathbf{k}}^1$  can realize two possible sets of valence bands:  $(\Gamma_5, K_3, M_3, M_4)$  or  $(\Gamma_6, K_3, M_1, M_2)$ , assuming, without loss of generality, that the  $K_3$  irrep appears in the valence bands instead of the conduction bands. (As noted at the end of the last section, there are two other disconnected phases listed in the BANDREP application that that our model does not realize and which differ in the  $C_{2z}$  eigenvalues of occupied bands; presumably they require longer range hopping). By comparing to the list of band representations induced from Wyckoff positions in  $P6mm$  (SG 183) (which describes layers of the honeycomb lattice with no additional symmetry in the  $z$  direction), we see that the irreps in  $A_1 \uparrow G$  or  $B_2 \uparrow G$  from the  $1a$  position are  $(\Gamma_1, K_1, M_1)$  or  $(\Gamma_3, K_1, M_3)$ , respectively, while the irreps in  $A_1 \uparrow G$  on the  $3c$  position are  $(\Gamma_1, \Gamma_5, K_1, K_3, M_1, M_3, M_4)$  and the irreps in  $B_1 \uparrow G$  on the  $3c$  position are  $(\Gamma_3, \Gamma_6, K_1, K_3, M_1, M_2, M_3)$ . Thus, we see that for each of the possible sets of valence bands in our model, the irreps that appear are obtained from subtracting the irreps of one of the EBRs induced from the  $1a$  position from one of the EBRs induced from the  $3c$  position. A classification scheme that only looks at the irreps at high-symmetry points will classify our valence bands as trivial. It was noted in Ref 4 that some topologically nontrivial bands will be included in the trivial class; our model is an example of this phenomenon.

## C. Phase diagram with SOC

Including SOC,  $\Gamma_5 \rightarrow \bar{\Gamma}_7 \oplus \bar{\Gamma}_8$ ,  $\Gamma_6 \rightarrow \bar{\Gamma}_7 \oplus \bar{\Gamma}_9$  and  $K_1 \rightarrow \bar{K}_6$ ,  $K_2 \rightarrow \bar{K}_6$ ,  $K_3 \rightarrow \bar{K}_4 \oplus \bar{K}_5 \oplus \bar{K}_6$ . Thus, the irreps that appear in a model with spinful  $p_{x,y}$  orbitals on the honeycomb lattice are

$$2\bar{\Gamma}_7 \oplus \bar{\Gamma}_8 \oplus \bar{\Gamma}_9 \text{ and } 3\bar{K}_6 \oplus \bar{K}_4 \oplus \bar{K}_5 \quad (\text{S14})$$

As mentioned in the main text, they belong to a sum of three EBRs,  ${}^1\bar{E} \uparrow G$ ,  ${}^2\bar{E} \uparrow G$ , and  $\bar{E}_1 \uparrow G$ , induced from the  $2b$  position. The double-valued EBRs for SG 183 are listed in Table S3. (Since there is only one double-valued irrep of the little group at  $M$ , it cannot be used to distinguish EBRs and we do not need to consider it here.) Since the  $\bar{E}_1 \uparrow G$  EBR is decomposable, generically, the band structure splits into four groups of bands. One possibility is that one branch contains the irreps  $\bar{\Gamma}_8$  and  $\bar{K}_6$ , another contains  $\bar{\Gamma}_9$  and  $\bar{K}_6$ , another contains  $\bar{\Gamma}_7$  and  $\bar{K}_6$  and the last contains  $\bar{\Gamma}_7$  and  $\bar{K}_4 \oplus \bar{K}_5$ . In this case, each branch has the same irreps at high-symmetry points as an EBR listed in Table S3, but the EBR might come from orbitals on the  $1a$  position. In the language of Ref 5, a branch that contains the same irreps as an EBR induced from orbitals located at a different site than the atoms is called an ‘‘obstructed atomic limit.’’ An obstructed

atomic limit can have localized Wannier functions, but since those Wannier functions are not located where the atoms are located, a gap must close in order to reach the phase where the Wannier functions and the atomic orbitals are localized at the same sites.

The other possibility is that the bands disconnect in such a way that some branches do not have the same irreps as an EBR; this can happen if a branch contains  $\bar{\Gamma}_8$  or  $\bar{\Gamma}_9$  and  $\bar{K}_4 \oplus \bar{K}_5$ . A branch that does not have the same irreps as an EBR does not correspond to an atomic limit and cannot yield maximally localized Wannier functions that obey the crystal symmetry, centered at any position.

Wyckoff	EBR	$\bar{\Gamma}$ irreps	$\bar{K}$ irreps	No. bands
$1a$	$\bar{E}_1 \uparrow G$	$\bar{\Gamma}_9$	$\bar{K}_6$	2
$1a$	$\bar{E}_2 \uparrow G$	$\bar{\Gamma}_8$	$\bar{K}_6$	2
$1a$	$\bar{E}_3 \uparrow G$	$\bar{\Gamma}_7$	$\bar{K}_4 \oplus \bar{K}_5$	2
$2b$	${}^1\bar{E} \uparrow G$	$\bar{\Gamma}_7$	$\bar{K}_6$	2
$2b$	${}^2\bar{E} \uparrow G$	$\bar{\Gamma}_7$	$\bar{K}_6$	2
$2b$	$\bar{E}_1 \uparrow G$	$\bar{\Gamma}_8 \oplus \bar{\Gamma}_9$	$\bar{K}_4 \oplus \bar{K}_5 \oplus \bar{K}_6$	4

TABLE S3. Double-valued EBRs in SG 183, obtained from the BANDREP application.<sup>3</sup>

When time-reversal symmetry is imposed, we can compute the  $\mathbb{Z}_2$  index. Let us first consider the case when SOC is spin-conserving; following Ref 5, we refer to this as ‘‘Haldane’’ SOC, as opposed to Rashba SOC, which, by our definition, is any SOC term that does not conserve spin. An SOC term that conserves spin will also preserve inversion symmetry (the inversion operator is exactly the tensor product of the spinless  $C_{2z}$  operator in Eq (S4) and the identity in spin space). We can compute the  $\mathbb{Z}_2$  index<sup>6</sup> from the product of  $C_{2z}$  eigenvalues at  $\Gamma$  and  $M$ , since each band in the spinless model gives rise to a Kramers pair with SOC, whose inversion eigenvalue is the same as the spinless  $C_{2z}$  eigenvalue. The eigenvalues of  $C_{2z}$  are given in Tables S1 and S2 and the product for each band is tabulated in Table S4 for all parameter regimes. (Note: there are three inequivalent  $M$  points, but they share the same  $C_{2z}$  eigenvalues). The ordered lists of  $C_{2z}$  eigenvalues in the last column of Table S4 reflect the particle-hole symmetry of our simplistic model; however, terms that break the particle-hole symmetry without inverting bands at  $\Gamma$  or  $M$  will not change the order of eigenvalues. The fact that some particle-hole symmetric arrangements do not appear (namely,  $+1, +1, +1, +1$  and  $+1, -1, -1, +1$ , is a surprising feature of our simple model.) Since the product of  $C_{2z}$  eigenvalues of the lowest band is always  $-1$ , whenever SOC opens a gap to the lowest energy band, it is a topological gap. If there is a gap at half-filling, there are two possibilities: if the gap was open before SOC was added, then the parameters  $t_{\sigma,\pi}$  are constrained by Eqs (S12)–(S13); comparing to Table S4 reveals that this gap will have a trivial  $\mathbb{Z}_2$  index (consistent with the fact that a spinless model must have a trivial  $\mathbb{Z}_2$  index.) On the other hand, in the parameter regime that violates

Eqs (S12)–(S13), the spinless system will be gapless at half-filling; if SOC opens a gap, then Table S4 shows that the gap has a nontrivial  $\mathbb{Z}_2$  index.

We now consider non-spin-conserving (Rashba) SOC and examine each of the high-symmetry points. First, Rashba SOC cannot open a gap at  $M$  since each spinless band is non-degenerate (when SOC is turned on, it will become a Kramers pair.) Second, Rashba SOC cannot open a gap at  $K$ : if two bands are degenerate at  $K$  in the spinless model, then they are in the  $K_3$  representation, which we showed in the supplement of Ref 5 (Sec IIID) can only be gapped if the strength of Haldane SOC exceeds that of Rashba SOC. Third, we examine the  $\Gamma$  point. In the spinless model, bands come in degenerate pairs, which are described by the  $\Gamma_5$  or  $\Gamma_6$  representation, where  $C_{2z}$  is represented by  $\pm\mathbb{I}$ . When we consider spin,  $C_{2z}$  is represented by  $\pm\mathbb{I} \otimes is_z$ , where  $s_z$  is the Pauli matrix describing the spin degrees of freedom. A term that breaks spin conservation will not commute with  $\mathbb{I} \otimes is_z$ . Hence, no Rashba term can appear at the  $\Gamma$  point because it will break  $C_{2z}$  symmetry. We conclude from examining all three high-symmetry points that any gap that is opened by small SOC is adiabatically related to a gap that is opened by spin-conserving SOC and hence the  $\mathbb{Z}_2$  topological index obtained from inversion eigenvalues still holds.

Parameter regime	Prod. $C_{2z}$ eigs.
$t_\pi < -t_\sigma \Rightarrow \begin{cases} E_{\Gamma 2} < E_{\Gamma 1} \\ E_{M 3} < E_{M 1} < E_{M 4} < E_{M 2} \end{cases}$	-1, +1, +1, -1
$t_\pi > 3t_\sigma \Rightarrow \begin{cases} E_{\Gamma 2} < E_{\Gamma 1} \\ E_{M 3, M 4} < E_{M 1, M 2} \end{cases}$	-1, -1, -1, -1
$t_\pi < -t_\sigma \Rightarrow \begin{cases} E_{\Gamma 2} < E_{\Gamma 1} \\ E_{M 4} < E_{M 2} < E_{M 3} < E_{M 1} \end{cases}$	-1, +1, +1, -1
$t_\pi > -t_\sigma \Rightarrow \begin{cases} E_{\Gamma 1} < E_{\Gamma 2} \\ E_{M 2} < E_{M 4} < E_{M 1} < E_{M 3} \end{cases}$	-1, +1, +1, -1
$t_\pi > \frac{1}{3}t_\sigma \Rightarrow \begin{cases} E_{\Gamma 1} < E_{\Gamma 2} \\ E_{M 1, M 2} < E_{M 3, M 4} \end{cases}$	-1, -1, -1, -1
$t_\pi > -t_\sigma \Rightarrow \begin{cases} E_{\Gamma 1} < E_{\Gamma 2} \\ E_{M 1} < E_{M 3} < E_{M 2} < E_{M 4} \end{cases}$	-1, +1, +1, -1

TABLE S4. Product of  $C_{2z}$  eigenvalues at  $\Gamma$  and  $M$  in order of increasing energy, for all possible parameter regimes. According to Eqs (S12) and (S13), the spinless model can only be gapped in the parameter regimes corresponding to the second or fifth row.

## S2. $d_{z^2}$ AND $d_{x^2-y^2}$ ORBITALS IN $P4_232$

Since the lattice of  $P4_232$  (SG 208) is primitive cubic, the lattice vectors are  $\mathbf{e}_1 = \hat{\mathbf{x}}, \mathbf{e}_2 = \hat{\mathbf{y}}, \mathbf{e}_3 = \hat{\mathbf{z}}$ . A unit cell is drawn in Fig. 3a; we take the origin to be one of the corners of the cube. Our model consists of

$d_{z^2}$  and  $d_{x^2-y^2}$  orbitals sitting at the corners and center of the cube. These orbitals transform as representations of  $T$  (generated by  $C_{2z}$  and  $C_{3,111}$ ), which is the “site-symmetry group” of the origin;<sup>7</sup> that is,  $T$  is the largest subset of  $P4_232$  that leaves the origin invariant. The  $d_{z^2}$  and  $d_{x^2-y^2}$  orbitals transform as the one-dimensional irreps,  ${}^1E$  and  ${}^2E$ , of  $T$ .<sup>8</sup> Since they are time-reversed partners, they transform as a single irrep under the symmetries of  $T$  and time-reversal. (We also note that the tensor product of the spin- $\frac{1}{2}$  representation with  $d_{z^2}$  and  $d_{x^2-y^2}$  orbitals yields the two-dimensional irreps,  ${}^1F_{3/2}$  and  ${}^2F_{3/2}$ .<sup>9</sup>) Instead of choosing the diagonal set of matrix representatives, we choose a physically motivated basis, where a rotation by an angle  $\theta$  about an axis  $\hat{\mathbf{n}}$  is represented by  $e^{i\theta\hat{\mathbf{n}}\cdot\mathbf{S}}$ , projected onto the  $d_{z^2}$  and  $d_{x^2-y^2}$  orbitals. This yields  $C_{2z} = C_{2x} = C_{2y} = \sigma_0$ , and

$$C_{3,111} = -\frac{1}{2}\mathbb{I} + \frac{\sqrt{3}}{2}(i\sigma_y) = \begin{pmatrix} -\frac{1}{2} & \frac{\sqrt{3}}{2} \\ -\frac{\sqrt{3}}{2} & -\frac{1}{2} \end{pmatrix} \quad (\text{S15})$$

The screw operation  $\tilde{C}_{2,110} \equiv \{C_{2,110}|\frac{1}{2}\frac{1}{2}\frac{1}{2}\}$  mixes the two sublattices consisting of sites at the origin and sites at the center,  $(\frac{1}{2}, \frac{1}{2}, \frac{1}{2})$ , of each unit cell. The full representation of the symmetry operations is given by:

$$\begin{aligned} U_{C_{2z}} &= U_{C_{2y}} = \tau_0 \otimes \sigma_0 \\ U_{C_{3,111}} &= \tau_0 \otimes \left(-\frac{1}{2}\sigma_0 + \frac{\sqrt{3}}{2}i\sigma_y\right) \\ U_{\tilde{C}_{2,110,\mathbf{k}}} &= e^{-\frac{i}{2}(k_x+k_y-k_z)}\tau_x \otimes \sigma_z, \end{aligned} \quad (\text{S16})$$

where the  $\tau$  matrices act in the sublattice space. Time-reversal is implemented by complex conjugation. Since the representation cannot be reduced without breaking time-reversal symmetry, it is “physically irreducible.”<sup>10</sup>

## S3. SYMMETRY CONSTRAINTS ON THE WILSON LOOP IN $P4_232$ (SG 208)

We show how the symmetries of  $P4_232$  constrain the  $z$ -directed Wilson loop defined in Eq. (1); we will always take the base point  $k_{z0} = 0$ . We will frequently utilize the transformation of the Wilson loop under a non-symmorphic unitary symmetry,  $\{D_g|(\delta_x, \delta_y, \delta_z)\}$ , such that  $D_g$  acts in momentum space by  $(k_\perp, k_z) \rightarrow (D_g k_\perp, -k_z)$ , then

$$\mathcal{W}_{(D_g k_\perp, k_{z0})} = e^{2\pi i \delta_z} \tilde{U}_g(k_\perp, k_{z0}) \mathcal{W}_{(k_\perp, -k_{z0})}^\dagger (\tilde{U}_g(k_\perp, k_{z0}))^\dagger, \quad (\text{S17})$$

where

$$[\tilde{U}_g(\mathbf{k})]_{nm} \equiv \langle u^n(D_g \mathbf{k}) | U_g | u^m(\mathbf{k}) \rangle \quad (\text{S18})$$

This is a variation of Eq (B19) in Ref 11 or Eq (D8) in Ref 12. If  $D_g$  does not invert  $k_z$ , then there is no dagger on  $\mathcal{W}$  on the right-hand side of Eq (S17).

### A. Wilson eigenvalues along $\bar{\Gamma} - \bar{X} - \bar{M} - \bar{Y} - \bar{\Gamma}$

Let us first consider the eigenvalues of the Wilson matrix at  $\bar{\Gamma}$ . Enforcing  $C_{2x}$  symmetry, (recall,  $U_{C_{2x}} = \mathbb{I}_{4 \times 4}$  from Eq (S16)), Eq (S18) shows that  $\tilde{U}_{C_{2x}}(\Gamma) = \mathbb{I}_{2 \times 2}$ ; then Eq (S17) yields  $\mathcal{W}_{(\bar{\Gamma},0)} = \mathcal{W}_{(\bar{\Gamma},0)}^\dagger$ . This forces the eigenvalues of  $\mathcal{W}_{(\bar{\Gamma},0)}$  to be real. Enforcing  $\tilde{C}_{2,110}$  symmetry (which has  $\delta_z = \frac{1}{2}$ ), Eq (S17) yields  $\mathcal{W}_{(\bar{\Gamma},0)} = -\tilde{U}_{\tilde{C}_{2,110}} \mathcal{W}_{(\bar{\Gamma},0)}^\dagger \tilde{U}_{\tilde{C}_{2,110}}^\dagger$ , which shows that the eigenvalues of  $\mathcal{W}_{(\bar{\Gamma},0)}$  must be equal to +1 and -1.

Along the segment  $\bar{\Gamma} - \bar{X}$ , even without knowing  $\tilde{U}_{C_{2x}}(\mathbf{k})$ , we can utilize Eq (S17) to deduce that the eigenvalues of  $\mathcal{W}_{(k_x,0,0)}$  are equal to those of  $\mathcal{W}_{(k_x,0,0)}^\dagger$ . Consequently, the eigenvalues of  $\mathcal{W}_{(k_x,0,0)}$  must either come in complex conjugate pairs or be real. However, since the eigenvalues of  $\mathcal{W}_{(0,0,0)}$  are +1 and -1, the eigenvalues of  $\mathcal{W}_{(k_x,0,0)}$  must also be fixed to +1 and -1 along the entire line, since there is no way for them to smoothly vary while satisfying the constraints of  $C_{2x}$ .

Applying the same logic along  $\bar{X} - \bar{M}$  and  $\bar{Y} - \bar{\Gamma}$  with  $C_{2y}$  symmetry shows that the eigenvalues of  $\mathcal{W}_{(\pi,k_y,0)}$  and  $\mathcal{W}_{(0,k_y,0)}$  must also be pinned to +1 and -1. Finally, applying  $C_{2x}$  to  $\bar{M} - \bar{Y}$  to the eigenvalues of  $\mathcal{W}_{(k_x,\pi,0)}$ , we deduce that the eigenvalues of the  $z$ -directed Wilson matrix are equal to +1 and -1 along the entire loop  $\bar{\Gamma} - \bar{X} - \bar{M} - \bar{Y} - \bar{\Gamma}$ .

### B. Protected band crossing along $\bar{\Gamma} - \bar{M}$

Applying Eq (S17) with  $\tilde{C}_{2,110}$  symmetry to the line  $\bar{\Gamma} - \bar{M}$  shows that the eigenvalues of  $\mathcal{W}_{(k,k,0)}$  are the same as the eigenvalues of  $-\mathcal{W}_{(k,k,0)}^\dagger$ ; hence, the eigenvalues of  $\mathcal{W}_{(k,k,0)}$  are either pure imaginary or come in pairs

$$\lambda(k), -\lambda(k)^* \quad (\text{S19})$$

We showed in Sec S3A that the eigenvalues of  $\mathcal{W}_{(0,0,0)}$  (and  $\mathcal{W}_{(\pi,\pi,0)}$ ) are +1 and -1; this rules out the first possibility and hence the eigenvalues of  $\mathcal{W}_{(k,k,0)}$  come in pairs  $(\lambda(k), -\lambda(k)^*)$ , which are degenerate when  $\lambda(k) = \pm i$ . We now show that such a degeneracy can occur without any fine-tuning and that the parity of the number of degeneracies between  $k = 0$  and  $k = \pi$  constitutes a topological invariant.

To see this, we rely on an anti-unitary symmetry of the Hamiltonian:  $\mathcal{A} \equiv \mathcal{T} \tilde{C}_{2,110}^{-1} C_{2z} = \mathcal{T} \{C_{2,110} | \frac{1}{2} \frac{1}{2} \frac{1}{2} \}$ , satisfying  $\mathcal{A}^2 = 1$ . Since  $\mathcal{A}$  leaves  $(k, k, k_z)$  invariant, the (antiunitary) generalization of Eq (S17) is:

$$\mathcal{W}_{(k,k,k_{z0})} = -\tilde{U}_A(k, k, k_{z0}) K \mathcal{W}_{(k,k,k_{z0})} K (\tilde{U}_A(k, k, k_{z0}))^\dagger, \quad (\text{S20})$$

where the minus sign comes from the fact that  $\mathcal{A}$  includes a  $\frac{1}{2}$  translation in the  $\hat{z}$  direction ( $e^{2\pi i \delta_z} = -1$ ),  $K$  is the complex conjugation operator, and

$$\left[ \tilde{U}_A(\mathbf{k}) \right]_{nm} \equiv \langle u^n(\mathbf{k}) | \mathcal{A} | u^m(\mathbf{k}) \rangle \quad (\text{S21})$$

Notice that  $(\tilde{U}_A K)^2 = \mathbb{I}_{2 \times 2}$ , from which it follows that  $\tilde{U}_A(\mathbf{k}) = e^{ib_0(\mathbf{k}) + ib(\mathbf{k})(\cos \theta(\mathbf{k})\sigma_x + \sin \theta(\mathbf{k})\sigma_z)}$ . Importantly,  $\sigma_y$  does not appear in the exponential. Consequently  $\tilde{U}_A$  is diagonalized by  $\tilde{U}_A(\mathbf{k}) = e^{ib_0(\mathbf{k})} O(\mathbf{k}) D(\mathbf{k}) O(\mathbf{k})^T$ , where  $O(\mathbf{k})$  is a real orthogonal matrix and  $D(\mathbf{k}) = \text{Diag}[e^{-ib(\mathbf{k})}, e^{ib(\mathbf{k})}]$ . Defining

$$W_k = O(k, k, 0)^T \mathcal{W}_{(k,k,0)} O(k, k, 0), \quad (\text{S22})$$

Eq (S20) yields

$$W_k = -D(k, k, 0) W_k^* D(k, k, 0)^* \quad (\text{S23})$$

Since  $W_k$  has the same eigenvalues as  $\mathcal{W}_{(k,k,0)}$ , whose eigenvalues must come in pairs given by Eq (S19),  $W_k$  can be written as

$$W_k = i e^{i\mathbf{a}(k) \cdot \boldsymbol{\sigma}} \quad (\text{S24})$$

for a smooth vector function  $\mathbf{a}(k) = (a_x(k), a_y(k), a_z(k))$ . Eq (S23) then places the following constraints at each  $\mathbf{k}$ :

$$a_z \sin |\mathbf{a}| = 0 = (a_y \sin b + a_x \cos b) \cos |\mathbf{a}| \quad (\text{S25})$$

Since  $\mathbf{a}(k)$  is a smoothly varying function, there are two possibilities: either  $\cos |\mathbf{a}(k)| = 0$  for all  $k$  (in which case the eigenvalues of  $W_k$  are fixed to  $\pm 1$ ) or  $\sin |\mathbf{a}(k)| \neq 0$ ,  $\cos |\mathbf{a}(k)| \neq 0$  except at isolated points, in which case,  $a_x(k) \propto a_y(k)$ ,  $a_z(k) = 0$ . (We rule out the case where  $\sin |\mathbf{a}(k)| = 0$  for all  $k$  because it is inconsistent with the fact that the eigenvalues of  $W_{k=0}$  are equal to  $\pm 1$ .) The condition  $a_x(k) \propto a_y(k)$ ,  $a_z(k) = 0$  means that degeneracies in the spectrum of  $W_k$  (and hence  $\mathcal{W}_{(k,k,0)}$ ) occur when  $a_x(k) = 0$ , which forces  $a_y(k) = 0$ . If such a degeneracy is present and linear in  $k$ , then it is not fine-tuned, in the sense that smoothly deforming  $a_x(k)$  will move the degeneracy, but not remove it; such degeneracies can only be removed pairwise.

Since at both  $\bar{\Gamma}$  and  $\bar{M}$ , the eigenvalues of  $W_k$  are fixed to +1 and -1, the parity of the number of linear crossings is a topological invariant, that cannot be changed without closing the gap in the bulk band spectrum. Returning to the possibility that  $\cos |\mathbf{a}(k)| = 0$  for all  $k$ : since in this case the eigenvalues of  $W_k$  are never degenerate, it trivially follows that the parity of linear in  $k$  band crossings cannot be changed without closing the bulk gap.

### C. Winding of the bent Wilson loop

The product of  $C_{2x}$  and  $\tilde{C}_{2,110}$  yields the screw symmetry,  $\tilde{C}_4 \equiv \{C_{4z} | \frac{1}{2} \frac{1}{2} \frac{1}{2}\}$ . Applying Eq (S17) with  $\delta_z = \frac{1}{2}$ , and removing the dagger on the righthand side of Eq (S17) because  $\tilde{C}_4$  leaves  $k_z$  invariant, requires that the eigenvalues of  $\mathcal{W}_{(k,k,k_{z0})}$  are exactly opposite those of  $\mathcal{W}_{(-k,k,k_{z0})}$ .

If there is an odd number of linear band crossings in the spectrum of  $\mathcal{W}_{(k,k,k_{z0})}$  for  $0 \leq k \leq \pi$ , then one band must

have eigenvalue  $e^{i\varphi(k)}$ , where  $\varphi(0) = 0$  and  $\varphi(\pi) = \pi$ . The eigenvalue of the other band is given by  $e^{i\pi-i\varphi(k)}$ , according to Eq (S20). Then  $\tilde{C}_4$  requires that one band of  $\mathcal{W}_{(-k,k,k_z)}$  has eigenvalue  $-e^{i\pi-i\varphi(k)} = e^{-i\varphi(k)}$ ; we use this band to define  $\varphi(k)$  when  $-\pi < k < 0$ , i.e.,  $\varphi(-k) = -\varphi(k)$ . Thus, if we plot  $\varphi(k)$  from  $-\pi < 0 < \pi$ , it “winds” from  $-\pi$  to  $\pi$ . This is exactly what is shown in Fig. 3b. Applying the same logic to the other band shows that it winds in the opposite direction.

#### S4. WILSON-OF-WILSON LOOP

Let  $C$  be the closed path in the surface Brillouin zone that traverses  $\bar{\Gamma} - \bar{X} - \bar{M} - \bar{Y} - \bar{\Gamma}$  and, for each  $k_\perp \in C$ , let  $|v_{1,2}(k_\perp)\rangle$  by the eigenstates of  $\mathcal{W}_{(k_\perp,0)}$  with energies  $-1$  and  $+1$ , respectively. We define the Berry phase of the Wilson loop (the “Wilson-of-Wilson” loop) by  $w = e^{i\oint_C dk_\perp a(k_\perp)}$ , where  $a(k_\perp) = i\langle v_1(k_\perp)|\partial_{k_\perp}|v_1(k_\perp)\rangle$ .

We show that the symmetry  $C_{2z}\mathcal{T}$  requires  $w = \pm 1$ . In analogy to Eq (S20), the Wilson matrix satisfies,

$$\mathcal{W}_{(k_\perp,0)} = \tilde{U}_{C_{2z}\mathcal{T}}(k_\perp,0)K\mathcal{W}_{(k_\perp,0)}^\dagger K\tilde{U}_{C_{2z}\mathcal{T}}(k_\perp,0)^\dagger, \quad (\text{S26})$$

where,

$$\left[\tilde{U}_{C_{2z}\mathcal{T}}(k_\perp, k_z)\right]_{nm} \equiv \langle u^n(k_\perp, -k_z)|C_{2z}\mathcal{T}|u^m(k_\perp, k_z)\rangle \quad (\text{S27})$$

When  $k_\perp \in C$ ,  $\mathcal{W}_{(k_\perp,0)}$  is Hermitian, as we showed in Sec S3 A. Hence,  $\tilde{U}_{C_{2z}\mathcal{T}}(k_\perp,0)K$  is an anti-unitary symmetry that commutes with  $\mathcal{W}_{(k_\perp,0)}$  and hence does not mix the two Wilson bands, which are gapped with eigenvalues  $\pm 1$  along  $C$ . Thus, Eq (S20) can be applied with  $\mathcal{W}$  replaced by  $w$ :

$$w = e^{i\phi(\bar{\Gamma})}KwKe^{-i\phi(\bar{\Gamma})} \quad (\text{S28})$$

and

$$e^{i\phi(k_\perp)} = \langle v_1(k_\perp)|\tilde{U}_{C_{2z}\mathcal{T}}(k_\perp)|v_1(k_\perp)\rangle, \quad (\text{S29})$$

Eq (S28) shows that  $w$  is real and equal to  $\pm 1$ .

\* Permanent Address: Department of Physics, Princeton University, Princeton, New Jersey 08544, USA

<sup>1</sup> J. C. Slater and G. F. Koster, Phys. Rev. **94**, 1498 (1954).

<sup>2</sup> A. Alexandradinata, X. Dai, and B. A. Bernevig, Physical Review B **89**, 155114 (2014).

<sup>3</sup> L. Elcoro, B. Bradlyn, Z. Wang, M. G. Vergniory, J. Cano, C. Felser, B. A. Bernevig, D. Orobengoa, G. de la Flor, and M. I. Aroyo, Journal of Applied Crystallography **50**, 1457 (2017), arXiv:1706.09272.

<sup>4</sup> H. C. Po, A. Vishwanath, and H. Watanabe, Nature Communications **8**, 50 (2017), arXiv:1703.00911.

<sup>5</sup> B. Bradlyn, L. Elcoro, J. Cano, M. G. Vergniory, Z. Wang, C. Felser, M. I. Aroyo, and B. A. Bernevig, Nature **547**, 298 (2017), arXiv:1703.02050 [cond-mat].

<sup>6</sup> L. Fu and C. L. Kane, Phys. Rev. B **76**, 045302 (2007).

<sup>7</sup> M. I. Aroyo, ed., *International Tables for Crystallography*, Vol. A (International Union of Crystallography, 2016).

<sup>8</sup> M. I. Aroyo, A. Kirov, C. Capillas, J. M. Perez-Mato, and H. Wondratschek, Acta Cryst. **A62**, 115 (2006).

<sup>9</sup> S. Altmann and P. Herzig, *Point-Group Theory Tables*, 2nd ed. (University of Vienna, 2011).

<sup>10</sup> M. I. Aroyo, J. M. Perez-Mato, D. Orobengoa, E. Tasci, G. de la Flor, and A. Kirov, Bulg. Chem. Commun. **43(2)**, 183 (2011).

<sup>11</sup> A. Alexandradinata, Z. Wang, and B. A. Bernevig, Phys. Rev. X **6**, 021008 (2016).

<sup>12</sup> B. J. Wieder, B. Bradlyn, Z. Wang, J. Cano, Y. Kim, H.-S. D. Kim, A. M. Rappe, C. L. Kane, and B. A. Bernevig, (2017), arXiv:1705.01617.